ADVANCED FUNCTIONAL MATERIALS
www.afm-journal.de

Vertical Orientation of Nanodomains on Versatile Substrates through Self-Neutralization Induced by Star-Shaped Block Copolymers

*Sangshin Jang, Kyuseong Lee, Hong Chul Moon, Jongheon Kwak, Jicheol Park, Gumhye Jeon, Won Bo Lee, and Jin Kon Kim**

Vertical orientation of lamellar and cylindrical nanodomains of block copolymers on substrates is one of the most promising means for developing nanopatterns of next-generation microelectronics and storage media. However, parallel orientation of lamellar and cylindrical nanodomains is generally preferred due to different affinity between two block segments in a block copolymer toward the substrate and/or air. Thus, vertical orientation of the nanodomains is only obtained under various pre- or post-treatments such as surface neutralization by random copolymers, solvent annealing, and electric or magnetic field. Here, a novel self-neutralization concept is introduced by designing molecular architecture of a block copolymer. Star-shaped 18 arm poly(methyl methacrylate)-*block*-polystyrene copolymers ((PMMA-*b*-PS)$_{18}$) exhibiting lamellar and PMMA cylindrical nanodomains are synthesized. When a thin film of (PMMA-*b*-PS)$_{18}$ is spin-coated on a substrate, vertically aligned lamellar and cylindrical nanodomains are obtained without any pre- or post-treatment, although thermal annealing for a short time (less than 30 min) is required to improve the spatial array of vertically aligned nanodomains. This result is attributed to the star-shaped molecular architecture that overcomes the difference in the surface affinity between PS and PMMA chains. Moreover, vertical orientations are observed on versatile substrates, for instance, semiconductor (Si, SiO$_x$), metal (Au), PS or PMMA-brushed substrate, and a flexible polymer sheet of polyethylene naphthalate.

1. Introduction

Directed self-assembly (DSA) of block copolymers has received a great attention on next generation nanolithography for microelectronics and data storage media due to low cost, high speed, and simplicity of the process.[1–5] Although vertical orientation of lamellar and cylindrical nanodomains of block copolymers on a substrate is desirable, parallel orientation is usually obtained in a thin film because of different affinity between two block segments in a block copolymer toward the substrate and/or air. To induce vertical orientation, diverse pre- or post-treatments to neutralize the preferential affinity have been introduced in the literature, for instance, solvent vapor annealing,[6–9] surface neutralization by random copolymer brush treatment,[10–12] blend system,[13] graphoepitaxy,[14,15] temperature gradient,[16,17] electric field[18,19] or top coating.[20–22] Among them, solvent vapor annealing is one of the most powerful post-treatment methods for developing vertical orientation of block copolymer nanodomains. However, this method is difficult to apply for industrial applications owing to the use of solvents and the dewetting problem. To avoid using solvent, thermal annealing of block copolymer thin films would be the most promising platform for commercialization of DSA due to easy and large scale process. However, to induce vertically oriented nanodomains, neutralization of a substrate by various surface modifications, for instance, functionalization with random copolymers, introducing rough substrates, employing graphene films or nanoparticle monolayers,[11,13,23–25] is still needed to tune interfacial interactions between a substrate and each block of the block copolymer. Therefore, a simple and cost-effective DSA process that does not require above-mentioned neutralization methods and solvent vapor annealing is demanded for the fabrication of vertically oriented nanodomains to compete with conventional top-down lithography.

Kramer and co-workers[26] investigated the effect of block copolymer chain architecture on the orientation of nanodomains in relatively thick films (600–800 nm) using poly(cyclohexylethylene)-*block*-poly(ethylene) (PCHE-*b*-PE) block copolymers. They found that PCHE-*b*-PE-*b*-PCHE triblock copolymer showed perpendicularly oriented nanodomains by introducing lower surface energy block as the midblock, whereas PCHE-*b*-PE diblock copolymer exhibited parallel

S. Jang, K. Lee, Dr. H. C. Moon, J. Kwak, J. Park, Dr. G. Jeon, Prof. J. K. Kim
National Creative Research Initiative Center for Smart Block Copolymer Self-Assembly
Department of Chemical Engineering
Pohang University of Science and Technology (POSTECH)
Pohang, Gyungbuk 790-784, South Korea
E-mail: jkkim@postech.ac.kr
Prof. W. B. Lee
School of Chemical and Biological Engineering
Seoul National University
Seoul 151-742, South Korea

DOI: 10.1002/adfm.201502006

orientation. The difference was explained by the self-consistent mean field theory that for a small difference in the surface energy between two blocks, the entropy penalty associated with the midblock looping in the surface wetting layer for the parallel orientation is larger than the enthalpic penalty arising between two blocks.[27]

To maximize the entropy penalty as well as the introduction of an easily etchable block, for instance, poly(methyl methacrylate) (PMMA), we designed 18 arm star-shaped poly(methyl methacrylate)-*block*-polystyrene copolymers ((PMMA-*b*-PS)$_{18}$), where PMMA and PS consist of core and shell. By using this star-shaped block copolymer, in this study, we introduce a novel self-neutralization method. Due to this unique molecular architecture, parallel orientation of nanodomains in a thin film gives a huge entropic penalty, which finally overcomes the favorable interaction of a substrate and one of the blocks, resulting in vertical orientation of nanodomains.

By employing (PMMA-*b*-PS)$_{18}$ with two different PS volume fractions (f_{PS} of 0.60 and 0.78 corresponding to lamellar and PMMA cylindrical nanodomains), we were able to develop vertically oriented lamellae and hexagonally packed cylinders on the substrate by spin-coating without using any pre- or post-treatment. Although as-spun film showed relatively poor spatial ordering of vertically aligned nanodomains, the spatial ordering was significantly improved by thermal annealing for a short time (less than 30 min). The grazing-incidence small-angle X-ray scattering and scanning electron microscopy studies revealed that nanodomains were vertically aligned across the entire film thickness. Moreover, vertically aligned lamellae or cylinders were achieved on diverse substrates including semiconductor (Si, SiO_x), metal (Au), PS and PMMA-brushed substrates, and a flexible polymer substrate of polyethylene naphthalate (PEN). This facile self-neutralization approach gives a new concept for fabrication of vertically oriented nanostructures, and it would greatly contribute toward commercialization of DSA.

2. Results and Discussion

The synthesis and molecular characterization of two star-shaped block copolymers with two different PS volume fractions (f_{PS}) (STAR-LAM with f_{PS} = 0.60 and STAR-CYL with f_{PS} = 0.78 showing lamellar and cylindrical nanodomains, respectively) are described in Section 1 of the Supporting Information. The domain spacing (L_0) of the lamellar and cylindrical nanodomains is 51 and 53 nm, respectively, measured by small angle X-ray scattering (Figure S4, Supporting Information).

2.1. Vertically Oriented Nanodomains of Star-Shaped Block Copolymer by Surface-Neutralization

Vertical orientation of lamellar and cylindrical nanodomains was induced during the spin-coating without thermal annealing, as shown in Figure S5, Supporting Information, but the spatial ordering of vertically aligned nanodomains was relatively poor. But, by performing thermal annealing at 180 °C for a short time (10 min for cylinders and 30 min for lamellae), the spatial ordering of vertically oriented nanodomains was much improved and similar to that annealed at 180 °C for a long time (24 h). In this study, all thin films were thermally annealed at 180 °C for 24 h to ensure the equilibrium morphology of the nanodomains.

Figure 1 shows phase contrast atomic force microscopy (AFM) images for STAR-LAM and STAR-CYL on a pristine silicon wafer after the samples were annealed at 180 °C for 24 h. The bright regions in AFM image represent PMMA nanodomains. The finger-printed patterns clearly indicate that thin films of STAR-LAM showed vertical orientation of lamellar nanodomains with various thicknesses (1.0–2.0 L_0) (Figure 1a–d).

It was reported that PS-*b*-PMMA diblock copolymer with lamellae and cylinders can even show vertical orientation on a substrate without any treatment.[28–30] This phenomenon,

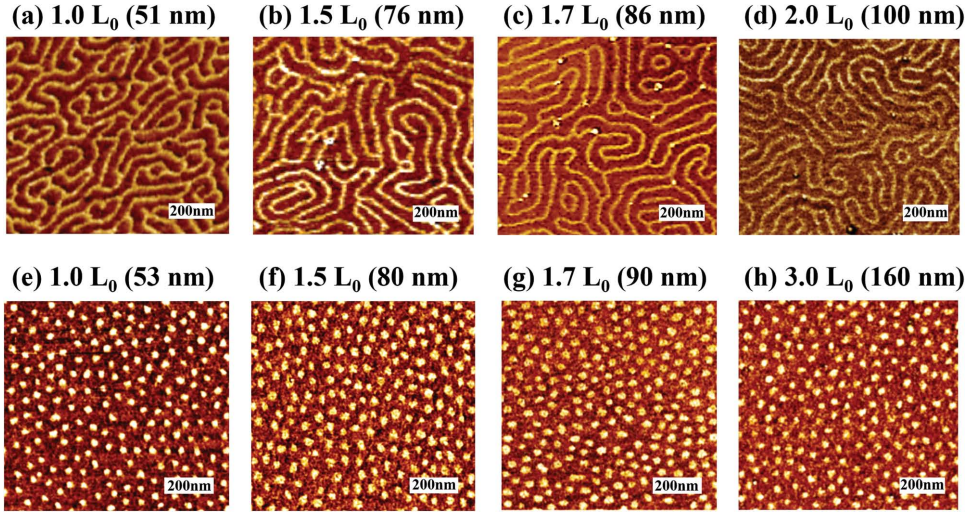

Figure 1. Phase contrast AFM images of STAR-LAM (f_{PS} = 0.60) thin film annealed at 180 °C for 24 h with various thicknesses: a) 1.0 L_0 (51 nm), b) 1.5 L_0 (76 nm), c) 1.7 L_0 (86 nm), d) 2.0 L_0 (100 nm). Phase contrast AFM images of STAR-CYL (f_{PS} = 0.78) thin film annealed at 180 °C for 24 h with various thicknesses: e) 1.0 L_0 (53 nm), f) 1.5 L_0 (80 nm), g) 1.7 L_0 (90 nm), h) 3.0 L_0 (160 nm).

however, was observed at a very limited thickness (for instance, close to 1.0 L_0 for silicon substrate with a native oxide). Furthermore, we found that vertical orientation of lamellar and cylindrical nanodomains of PS-*b*-PMMA diblock copolymers were not achieved for various substrates such as PS-brushed substrates or gold substrates, which are preferential for the PS block, as shown in Figure S6, Supporting Information, even though the film thickness is close to 1.5 L_0 which is the most appropriate thickness for the vertical orientation.

On the other hand, we obtained vertically oriented PMMA cylindrical nanodomains at various film thicknesses (1.0–3.0 L_0), as shown in Figure 1e–h. While the hexagonal packing of vertically oriented cylindrical nanodomains is not perfect, we obtain much better hexagonal packing of cylindrical nanodomains once a lithographically patterned silicon template (the width of 150 nm and the depth of 50 nm) was employed to utilize graphoepitaxy of STAR-CYL within the trench (see Figure S7, Supporting Information).

To confirm whether vertically oriented lamellar and cylindrical nanodomains span the entire film thickness, grazing-incidence small-angle X-ray scattering (GISAXS) experiments were performed. **Figure 2**a,c shows GISAXS patterns of STAR-LAM and STAR-CYL at an incident angle of 0.16°. As shown in Figure 2a, sharp vertical streaks (Bragg rod) were observed at the first-order reflection (q_{xy} = 0.123 nm^{-1}) which comes from lamellar nanodomains oriented normal to the surface across the entire thickness. In-plane scattering profile extracted at q_z = 0.277 nm^{-1} shows higher-order peaks at the integers (2, 3, 4, and 5) of q^*, indicating that thin film of STAR-LAM has lamellar nanodomains (Figure 2b). We also observed from Figure 2c sharp vertical streaks at the first-order reflection (q_{xy} = 0.120 nm^{-1}), indicating cylindrical nanodomains oriented normal to the surface. In-plane scattering profile extracted at q_z = 0.285 nm^{-1} in Figure 2d shows higher-order peaks at $\sqrt{3}q^*$, $\sqrt{7}q^*$, indicating that thin film of STAR-CYL has cylindrical nanodomains.

Figure 3a gives cross-sectional scanning electron microscopy (SEM) images of STAR-LAM after the removal of PMMA block by UV-etching followed by acetic acid rinsing. Vertically oriented PS lamellae are well maintained through the entire film thickness after the removal of PMMA block. Also, vertically oriented cylindrical nanoporous structure was obtained from air surface to the bottom of the substrate after the removal of PMMA block (Figure 3b).

2.2. Vertical Orientation of (PMMA-*b*-PS)$_{18}$ on Diverse Substrates

To demonstrate vertical orientation of (PMMA-*b*-PS)$_{18}$ on diverse substrates, both of PS and PMMA chains were grafted on a pristine silicon wafer by using hydroxy-terminated PS (PS-OH) and PMMA (PMMA-OH).[31] Vertically oriented lamellar and cylindrical nanodomains were obtained even on PS (and PMMA)-brushed silicon substrate (Figure S8, Supporting Information).

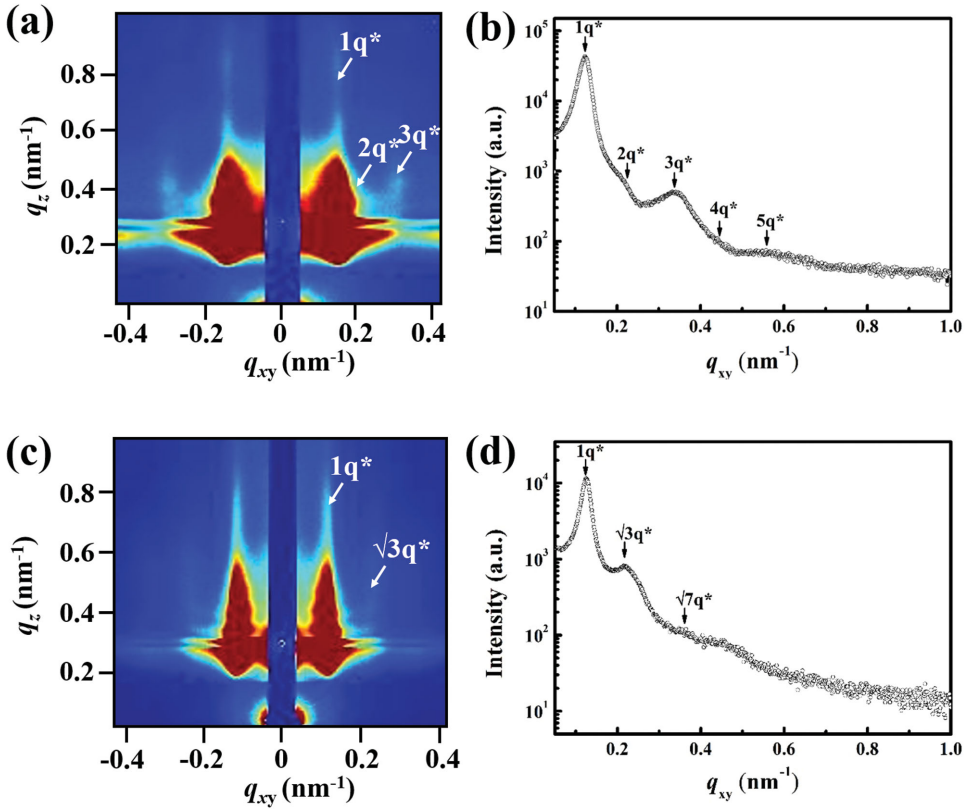

Figure 2. GISAXS patterns at an incident angle of 0.16° on pristine silicon wafer for a) STAR-LAM and c) STAR-CYL thin films. The in-plane scans for b) STAR-LAM at q_z = 0.277 nm^{-1} and d) STAR-CYL at q_z = 0.285 nm^{-1}.

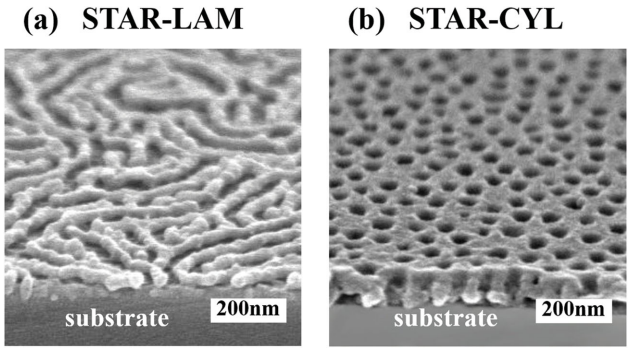

Figure 3. Cross-sectional SEM images of a) STAR-LAM and b) STAR-CYL on silicon wafer with a native oxide layer after the removal of PMMA block by UV irradiation, followed by rinsing with acetic acid.

Finally, we used two other substrates: a flexible polymer substrate and a gold-coated conducting substrate. Flexible substrates are very important in wearable electronic devices.[32,33] Here, we chose PEN substrate with a good strength, modulus and high chemical hydrolytic resistance; thus, it would be one of the best candidates for flexible integrated circuits. PEN substrate was easily bent without breaking, as shown in **Figure 4**a. Figure 4b,c is phase-contrast AFM images of STAR-LAM and STAR-CYL coated on PEN substrate. It is clearly shown that vertically oriented lamellar and cylindrical nanodomains were successfully obtained even after bending 10 times the PEN substrate. It was also confirmed that vertically oriented lamellar and cylindrical nanostructures were maintained from top to bottom after the removal of PMMA block by UV-etching on the PEN substrate (Figure S9, Supporting Information). Moreover, vertically oriented lamellar and cylindrical nanodomains are obtained on gold (Au) substrate, a representative conducting substrate, as shown in Figure 4d,e.

2.3. Mechanism for Vertically Oriented Nanodomains of Star-Shaped Block Copolymer

Vertically aligned nandomains were maintained even for ≈2.0 L_0 for STAR-LAM (Figure 1d) and ≈3.0 L_0 for STAR-CYL (Figure 1h). We consider why vertical orientation of nanodomains in star-shaped block copolymer thin film was obtained regardless of substrates. Here, inner (PMMA) and outer (PS) block chains of star-shaped block copolymer have preferential affinity with substrate and air, respectively. Parallel orientation of nanodomains is preferential in thin film of linear type block copolymer due to different affinity between two block segments toward the substrate (**Figure 5**a,b). In this case, one of the block segments having preferential affinity with the substrate is located at the substrate. However, the arrangement of star-shaped block copolymer molecules on a substrate is dramatically different from that of linear type block copolymer due to the existence of numerous covalently linked junction points.

Figure 5c–f gives schematic self-assembly for lamellar and cylindrical nanodomains of star-shaped block copolymers on a substrate with 1.5 L_0 thickness. For the formation of parallel oriented lamellar nanodomains of star-shaped block copolymer, inner block chains must be in contact with substrate due to the preferential affinity by arranging chains

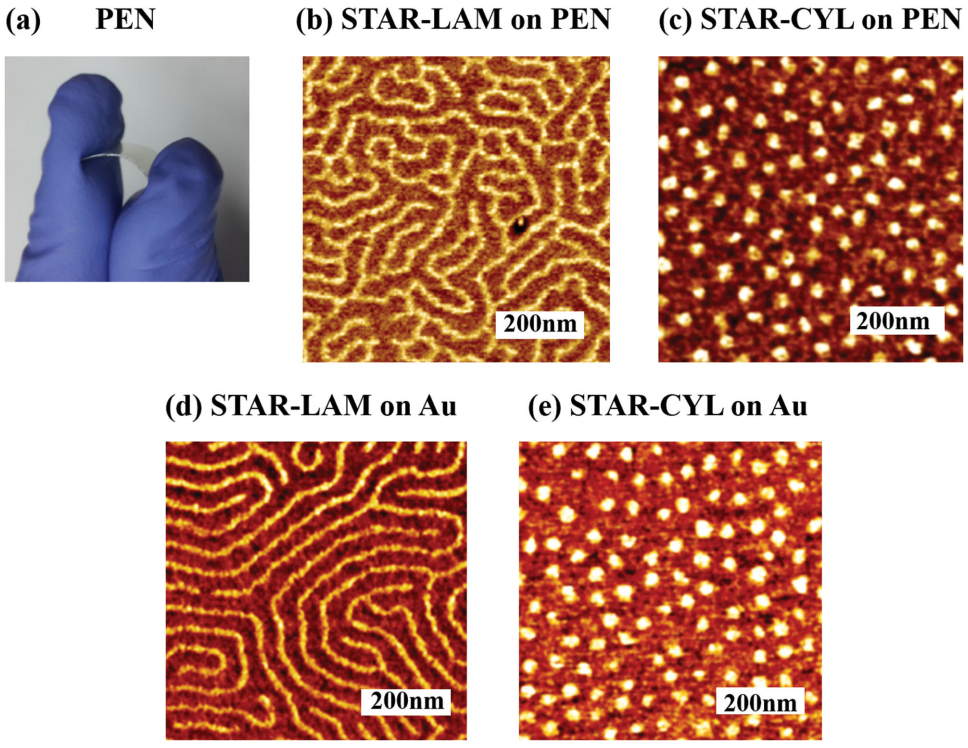

Figure 4. a) Photograph of bent PEN substrate. Phase contrast AFM images of b) STAR-LAM and c) STAR-CYL thin films on PEN substrate after PEN was bent 10 times. Phase contrast AFM images of d) STAR-LAM and e) STAR-CYL thin films on Au substrate.

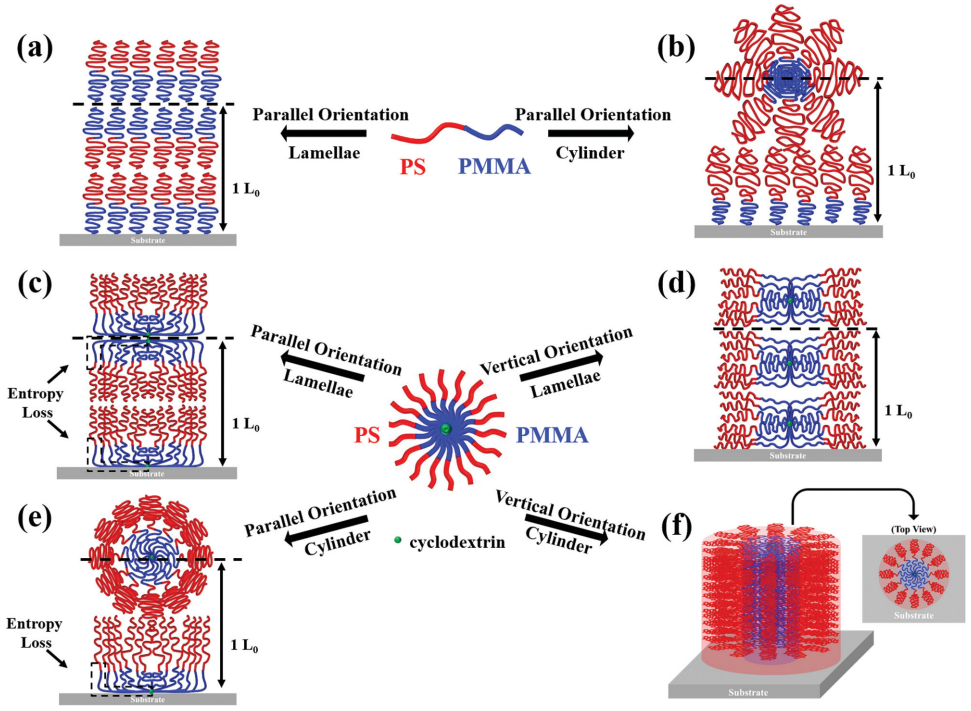

Figure 5. Chain arrangement of linear diblock copolymer on a substrate with thickness of 1.5 L_0 for a) lamellar and b) cylindrical nanodomains. Chain arrangement of lamellar nanodomains of star-shaped block copolymer on a substrate with thickness of 1.5 L_0 for c) parallel and d) vertical orientations. Chain arrangement of cylindrical nanodomains of star-shaped block copolymer on a substrate for e) parallel and f) vertical orientations.

into one direction (Figure 5c). In this case, to cover fully the substrate, the chains located far from the junction point are much more stretched compared to other chains located near the junction point, causing a large entropy loss. This entropy loss would be significantly greater than enthalpy gain by preferential interaction between one of block segments and the substrate, which is a dominant factor for linear diblock copolymer.

Therefore, the chains tethered at the junction point could aggregate along two directions parallel to the substrate surface, resulting in vertical orientation, as shown in Figure 5d. It is quite obvious that the chains for the vertical orientation are much less stretched compared to a parallel orientation. The reduced entropy loss arising from star-shaped molecular architecture can play a key role as self-neutralization on a substrate, resulting in vertical orientation of lamellar nanodomains.

For the formation of parallel oriented cylindrical nanodomains of star-shaped block copolymer, inner block chains must cover the substrate due to the preferential affinity (Figure 5e). Similarly to parallel oriented lamellar nanodomains of star-shaped block copolymer, the chains located far from the junction point are much more stretched compared to other chains located near the junction point, causing a large entropy loss. Thus, each domain is piled up vertically on a substrate without stretching, resulting in vertical orientation (Figure 5f). It is very interesting to find the critical number of arms, via experiment or theory based on self-consistent field theory, for inducing vertical orientation from parallel orientation, but it would be a future work.

3. Conclusion

In conclusion, we were able to develop vertically oriented lamellar and cylindrical nanodomains by using 18 arm star-shaped (PMMA-*b*-PS)$_{18}$ through controlling the molecular architecture. Without solvent annealing or neutralization process of a substrate, vertically oriented lamellar and cylindrical nanodomains were successfully fabricated on various substrates, ranging from semiconductor (Si, SiO_x) to metal (Au), polymer brushed substrates, and a flexible polymer substrate. GISAXS and SEM confirmed that vertically oriented nanodomains span throughout the entire film thickness. This novel self-neutralization approach containing etchable PMMA block suggests a new concept for fabrication of vertically oriented nanostructures, and it would greatly contribute toward commercialization of DSA for next-generation integrated circuit and data storage media. It would be also very interesting whether the nanodomains in block copolymers having high χ such as polystyrene-*block*-poly(4-vinyl pyridine) or polystyrene-*block*-poly(dimethyl siloxane) that could provide sub 10 nm spacing, could be aligned vertically by controlling molecular architecture, but this is also a future work.

4. Experimental Section

Synthesis of (PMMA-b-PS)$_{18}$: Lamellae-forming (STAR-LAM) and cylinder-forming (STAR-CYL) star-shaped block copolymers were synthesized by atom transfer radical polymerization (ATRP) (see Section 1 in the Supporting Information).[34] Briefly, 18 hydroxy groups on α-cyclodextrin (α-CD) were replaced by bromine groups (Br-CD) through the esterification with 2-bromoisobutyryl bromide[35] to be used

as an initiator. Atom transfer radical polymerization (ATRP) of methyl methacrylate (MMA), followed by styrene (St), was performed at 90 °C after degassing by three freeze-thaw cycles to synthesize (PMMA-*b*-PS)$_{18}$ with copper bromide (I) (CuBr) and 2,2′-bipyridiyl (bip) as catalyst. The molar ratio of MMA (or St):Br-CD (or CD-(PMMA)$_{18}$):CuBr:bip = 500:1:1:2. The molecular weight of polymers was controlled by reaction time.

Thin Film Preparation: All thin films were prepared by spin-coating of 1.0–2.0 wt% toluene solution of STAR-LAM and STAR-CYL by changing rotating speed (rpm) to adjust film thickness on a pristine silicon wafer, PS or PMMA-brushed silicon wafer, and PEN substrate. Gold (Au) substrate was prepared via sputtering 10 nm Ti on a silicon substrate, followed by thermal evaporation of 100 nm Au. Lithographically patterned silicon template (trench) was prepared by conventional deep UV lithography and plasma etching techniques.[36] Finally, all the films were dried in a vacuum at room temperature and then annealed at 180 °C with various time from 0 to 30 min.

Characterization of Thin Film: Surface morphology and cross-sectional structure of thin film were observed by atomic force microscopy in the tapping mode (AFM, Veeco DI Dimension 3100 with Nanoscope V), field-emission scanning electron microscopy (SEM, Hitachi, S4800) operating at 3 kV. Cross-sectional SEM image for thin films was obtained after UV irradiation followed by rinsing with acetic acid (UV-etching) to remove the PMMA block. GISAXS experiments were performed at room temperature on beam line 3C at the Pohang Accelerator Laboratory (PAL) (Korea) to investigate the morphology of thin film through the entire thickness. The operating wavelength was 0.15 nm and a sample-to-detector distance was 3 m. The incident angle (α_i) was set at 0.16°, which is above the critical angle (0.14°) of (PMMA-*b*-PS)$_{18}$ thin film.

SAXS experiments were performed at room temperature on beam line 4C at the Pohang Accelerator Laboratory (PAL) (Korea), with a wavelength of 0.1608 nm. The sample-to-detector distance was 3 m. Sample was annealed at 180 °C for 24 h, followed by rapid quenching to liquid nitrogen. Thickness of the sample was 1.0 mm and the exposure time was 10 s.

Supporting Information

Supporting Information is available from the Wiley Online Library or from the author.

Acknowledgements

This work was supported by the National Creative Research Initiative Program supported by the National Research Foundation of Korea (2013R1A3A2042196). GISAXS measurements were carried out at Beamline 3C of the Pohang Accelerator Laboratory.

Received: May 15, 2015
Revised: July 2, 2015
Published online: July 30, 2015

[1] M. Park, C. Harrison, P. M. Chaikin, R. A. Register, D. H. Adamson, *Science* **1997**, *276*, 1401.
[2] I. Bita, J. K. W. Yang, Y. S. Jung, C. A. Ross, E. L. Thomas, K. K. Berggren, *Science* **2008**, *321*, 939.
[3] C. T. Black, K. W. Guarini, Y. Zhang, H. J. Kim, J. Benedict, E. Sikorski, I. V. Babich, K. R. Milkove, *IEEE Electron Device Lett.* **2004**, *25*, 622.
[4] A. Jo, W. C. Joo, W.-H. Jin, H. Nam, J. K. Kim, *Nat. Nanotechnol.* **2009**, *4*, 727.
[5] Y. S. Kim, H. Han, Y. S. Kim, W. Lee, M. Alexe, S. Baik, J. K. Kim, *Nano Lett.* **2010**, *10*, 2141.
[6] S. H. Kim, M. J. Misner, T. Xu, M. Kimura, T. P. Russell, *Adv. Mater.* **2004**, *16*, 226.
[7] S. H. Han, V. Pryamitsyn, D. Bae, J. Kwak, V. Ganesan, J. K. Kim, *ACS Nano* **2012**, *6*, 7966.
[8] E. Kim, H. Ahn, S. Park, H. Lee, M. Lee, S. Lee, T. Kim, E.-A. Kwak, J. H. Lee, X. Lei, J. Huh, J. Bang, B. Lee, D. Y. Ryu, *ACS Nano* **2013**, *7*, 1952.
[9] S. W. Hong, W. Gu, J. Huh, B. R. Sveinbjornsson, G. Jeong, R. H. Grubbs, T. P. Russell, *ACS Nano* **2013**, *7*, 9684.
[10] P. Mansky, Y. Liu, E. Huang, T. P. Russell, C. Hawker, *Science* **1997**, *275*, 1458.
[11] E. Huang, T. P. Russell, C. Harrison, P. M. Chaikin, R. A. Register, C. J. Hawker, J. Mays, *Macromolecules* **1998**, *31*, 7641.
[12] D. Y. Ryu, K. Shin, E. Drockenmuller, C. J. Hawker, T. P. Russell, *Science* **2005**, *308*, 236.
[13] D. U. Ahn, E. Sancaktar, *Adv. Funct. Mater.* **2006**, *16*, 1950.
[14] H.-D. Koh, Y. J. Park, S.-J. Jeong, Y.-N. Kwon, I. T. Han, M.-J. Kim, *J. Mater. Chem. C* **2013**, *1*, 4020.
[15] J. Y. Cheng, C. A. Ross, H. I. Smith, E. L. Thomas, *Adv. Mater.* **2006**, *18*, 2505.
[16] J. Bodycomb, Y. Funaki, K. Kimishima, T. Hashimoto, *Macromolecules* **1999**, *32*, 2075.
[17] R. J. Albalak, E. L. Thomas, M. S. Capel, *Polymer* **1998**, *38*, 3819.
[18] T. L. Morkved, M. Lu, A. M. Urbas, E. E. Ehrichs, H. M. Jaeger, P. Mansky, T. P. Russell, *Science* **1996**, *273*, 931.
[19] T. Thurn-Albrecht, J. Schotter, G. A. Kästle, N. Emley, T. Shibauchi, L. Krusin-Elbaum, K. Guarini, C. T. Black, M. T. Tuominen, T. P. Russell, *Science* **2000**, *290*, 2126.
[20] C. M. Bates, T. Seshimo, M. Maher, W. J. Durand, J. D. Cushen, L. M. Dean, G. Blachut, C. J. Ellison, C. G. Wilson, *Science* **2012**, *338*, 775.
[21] M. J. Maher, C. M. Bates, G. Blachut, S. Sirard, J. L. Self, M. C. Carlson, L. M. Dean, J. D. Cushen, W. J. Durand, C. O. Hayes, C. J. Ellison, C. G. Wilson, *Chem. Mater.* **2014**, *26*, 1471.
[22] a) E. Kim, W. Kim, K. H. Lee, C. A. Ross, J. G. Son, *Adv. Funct. Mater.* **2014**, *24*, 6981; b) E. Yoon, E. Kim, D. Kim, J. G. Son, *Adv. Funct. Mater.* **2015**, *25*, 913.
[23] E. Sivaniah, Y. Hayashi, M. Iino, T. Hashimoto, K. Fukunaga, *Macromolecules* **2003**, *36*, 5894.
[24] B. H. Kim, J. Y. Kim, S-J. Jeong, J. O. Hwang, D. H. Lee, D. O. Shin, S.-Y. Choi, S. O. Kim, *ACS Nano* **2010**, *4*, 5464.
[25] T. Kim, S. Wooh, J. G. Son, K. Char, *Macromolecules* **2013**, *46*, 8144.
[26] J. Ruokolainene, G. H. Fredrickson, E. J. Kramer, C. Y. Ryu, S. F. Hahn, S. N. Magonov, *Macromolecules* **2002**, *35*, 9391.
[27] V. Khanna, E. W. Cochran, A. Hexemer, G. E. Stein, G. H. Fredrickson, E. J. Kramer, X. Li, S. F. Hahn, *Macromolecules* **2006**, *39*, 9346.
[28] H. Wang, A. B. Djurišić, M. H. Xie, W. K. Chan, O. Kutsay, *Thin Solid Films* **2005**, *488*, 329.
[29] T. L. Morkved, H. M. Jaeger, *Europhys. Lett.* **1997**, *40*, 643.
[30] H.-C. Kim, T. P. Russell, *J. Polym. Sci., Part B: Polym. Phys.* **2001**, *39*, 663.
[31] R. Guo, E. Kim, J. Gong, S. Choi, S. Ham, D. Y. Ryu, *Soft Matter* **2011**, *7*, 6920.
[32] S. R. Forrest, *Nature* **2004**, *428*, 911.
[33] Z. Fan, H. Razavi, J.-W. Do, A. Moriwaki, O. Ergen, Y.-L. Chueh, P. W. Leu, J. C. Ho, T. Takahashi, L. A. Reichertz, S. Neale, K. Yu, M. Wu, J. W. Ager, A. Javey, *Nat. Mater.* **2009**, *8*, 648.
[34] S. Jang, H. C. Moon, J. Kwak, D. Bae, Y. Lee, J. K. Kim, W. B. Lee, *Macromolecules* **2014**, *47*, 5295.
[35] F. A. Plamper, H. Becker, M. Lanzendörfer, M. Patel, A. Wittemann, M. Ballauff, A. H. E. Müller, *Macromol. Chem. Phys.* **2005**, *206*, 1813.
[36] C. T. Black, O. Bezencenet, *IEEE Trans. Nanotechnol.* **2004**, *3*, 412.